

Three-Dimensional Stress Analysis around Rivet Holes in a Plate Subjected to Biaxial Loading

Ahmad S. Alshyyab^{*}, Feras H. Darwish

Aeronautical Engineering Department, Jordan University of Science and Technology, Irbid, 22110, Jordan

Received 6 September. 2018

Abstract

The three-dimensional (3-D) stress domain around a countersunk hole in an isotropic plate is exclusively dictated by the dimensions of the hole and its size relative to the plate when subjected to a uniaxial load. The application of a biaxial load would certainly redistribute the stresses around the hole. In this respect, the present research aims to investigate through finite element analysis (FEA) the effect of the biaxial remote stress ratio (R) on the in-plane stress concentration factors (SCF) and the out-of-plane stress constraint factor (C) in the vicinity of a countersunk hole. A finite element code is written by using ANSYS Parametric Design Language (APDL) and is used to build the FE model, apply the boundary conditions, and perform the analysis. Based on the FE results, it is found that the SCF decreases linearly with increasing the biaxial load ratio. It is also found that the maximum value of the stress constraint factor C_{max} is located at the straight shank part of the hole and its magnitude is bounded by zero for plane stress and one for plane strain.

© 2018 Jordan Journal of Mechanical and Industrial Engineering. All rights reserved

Keywords: countersunk hole, biaxial loading, finite element analysis, stress concentration factor, stress constraint factor;

1. Introduction

In industrial applications, structural components are normally joined together to form larger assemblies. Riveting is one type of the joining methods that is commonly used in aircraft and marine vessel industries. In this aspect, flush rivets are usually used when aerodynamic smoothness of the external surfaces of the structure is required. Upon their application, flush rivets form countersunk holes through the thickness of the joint. During the service life of such joints, countersunk holes act like stress risers at which micro cracks are likely to nucleate and propagate under different loading conditions. Therefore, stress and strain analyses around such holes should be carefully considered in the design process to reduce the risk of any premature failures and to enhance the strength of the joint.

Numerous studies on the SCF due to notches and holes of different geometries and under different loading conditions are reported in the literature [1]. The failure due to biaxial tensile loading of a quasi-isotropic composite plate with a circular hole was experimentally investigated [2, 3]. General stress functions were obtained to determine the SCF around cutouts in infinite composite laminates subjected to biaxial loading [4]. The upper and lower bounds of the limit loads of plates with elliptical and circular holes under uniaxial and biaxial loading conditions were estimated analytically and compared with

the finite element results [5]. A general analytical solution was also obtained for the stresses and deformations around a traction free elliptic hole in an infinite elastic plate subjected to a biaxial load [6]. Experimental failure test results of riveted fuselage lap joint specimens under uniaxial and biaxial loading conditions were reported by the FAA [7]. A finite element investigation was carried out on a stiffened plate with a square cutout under various combinations of biaxial loading conditions [8]. The local stresses around a plane hole in an aluminum specimen were determined experimentally by the birefringent-plastic coating method [9]. The effect of the dimensions of a countersunk hole on the SCF in infinite plates subjected to different types of loading conditions was investigated through finite element analysis [10]. Parametric equations for the stress and strain concentration factors around a countersunk hole in an isotropic plate under uniaxial tension were formulated based on regression analysis of the finite element results [11, 12]. A modified equation for the uniaxial SCF around a countersunk hole was reported as well [13]. A new equation for the SCF around countersunk rivet holes in orthotropic laminated plates subjected to uniaxial load was introduced as a function of the hole and plate geometries and the material orthotropy [14]. The SCF around circular holes in isotropic and orthotropic plates and pressure vessels was investigated through finite element analysis [15]. Finite element investigation of the in-plane stresses generated around two adjacent countersunk holes in isotropic plates subjected to

^{*} Corresponding author e-mail: asalshyyab@just.edu.jo.

uniaxial tension was performed [16]. The results revealed that an increase in the stress concentration occurs as the distance between the holes gets smaller. Analytical solutions for the three-dimensional stress domain around circular and non-circular holes in isotropic plates were presented. It was also shown that the out of plane stress constraint factor depends on the thickness of the plate [17]. A review study showed that there is a strong relevance between the plate thickness which affects the stress constraint factor at the notch and the brittle fracture of the plate components [18]. Three-dimensional finite element study was performed to investigate the elastic notch root fields for plates with different thicknesses and different notch configurations [19]. The effect of the plate thickness and the notch configuration on the SCF, the stress constraint factor and the strain energy density were studied through an analytical solution of the stress domain around the notch [20]. The finite element method was used to study the thorough thickness variation of the SCF along the wall of an elliptic hole in an isotropic plate under tension [21].

The main objective of this research is to study the combined effect of the biaxial stress ratio and the hole configuration on the in-plane SCF and the out-of-plane stress constraint factor at the countersunk hole in an isotropic plate.

2. The geometric model and the boundary conditions

Fig. 1 presents a 3-D illustration of the geometric model of a plate made of an isotropic and homogeneous material and accommodates a centered countersunk hole. The Cartesian x - y - z coordinates are used as a reference frame located at the bottom center of the hole. The plate has a length of $2L$, a width of $2w$ and a thickness t . The straight shank (SS) part of the hole has a radius and thickness of r and b respectively. The largest radius of the countersunk hole r_c is determined by the sinking depth C_s and the countersink angle θ_c . Biaxial remote tension stresses σ_{x0} and σ_{y0} are applied at the boundaries of the plate as shown.

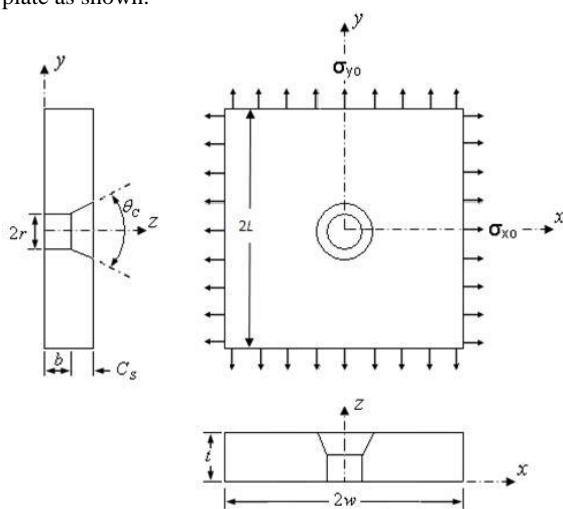


Figure 1. The geometry and boundary conditions of a plate with a centered countersunk hole

Due to the symmetry in the plate's geometry and in the applied stresses across the x - and y -axes, only one quarter of the configuration will be considered for the FE

modeling to reduce the number of generated nodes and elements and accordingly to reduce the analysis running time. Fig. 2 shows the split lines and one quarter of the plate. The new generated boundary conditions at the cut line (lines of symmetry) restrain the displacement in the x -direction at the surface at $x=0$ and the displacement in the y -direction at the surface at $y=0$. To suppress the rigid mode of body motion in the z -direction, the z -displacement of a one node located at $z = x = 0$ and $y = r$ was restrained.

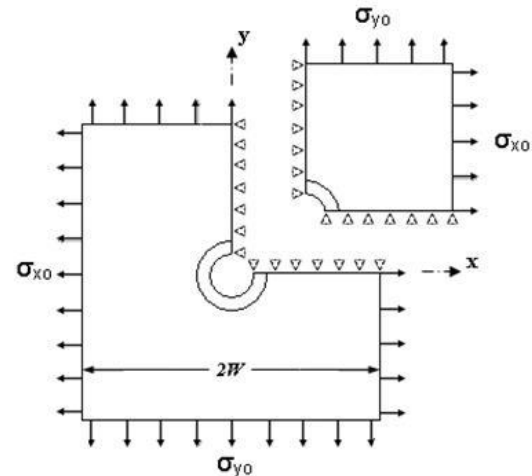


Figure 2. One quarter of the plate and the hole and the resulting boundary conditions

3. Finite Element Modeling

A commercial FEA code, ANSYS Version 13, was used to perform the analysis of the problem. In this respect, APDL batch code was written to generate the FE model, apply the boundary conditions, conduct the solution, and postprocess the results. Three-dimensional solid45 element type was used to generate -through isoperimetric mapping option- the elemental mesh domains for the volumes of the model. Mesh gradation and mesh refinement studies were carefully conducted to generate fine mesh domains at the regions of high stress gradients. The two studies were based on examining the convergence of the solution for different mesh upgrades to assure the accuracy of the results. Fig. 3 illustrates the typical mesh used in the analysis. The number of mesh elements and nodes were 44100 and 48564, respectively.

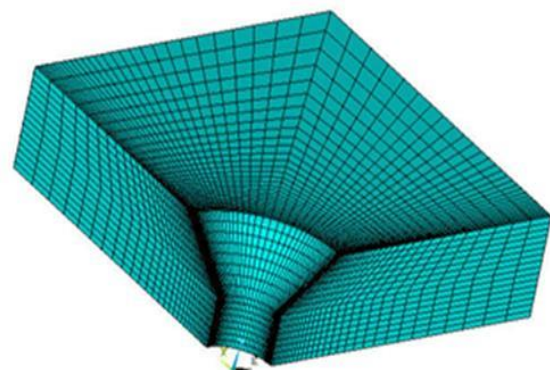


Figure 3. Typical mesh idealization used in the analysis.

In another aspect, as the region around the countersunk hole is expected to experience elevated stresses upon load application, the FE code is designed to save the desired stress results in this region along five paths of interest. As shown in Fig. 4, the five paths are: (i) path *ABC* formed by the intersection of the hole bore with the *x-z* plane at *y* = 0, (ii) path *DEF* formed by the intersection of the hole bore with the *y-z* plane at *x* = 0, (iii) circular path *CF* of radius *r_c* formed by the intersection of the hole bore with the *x-y* plane at *z* = *t* and (iv, v) two circular paths *AD* and *BE* formed by the intersections of the hole bore with *x-y* plane at *z* = 0 and *z* = *b*, respectively.

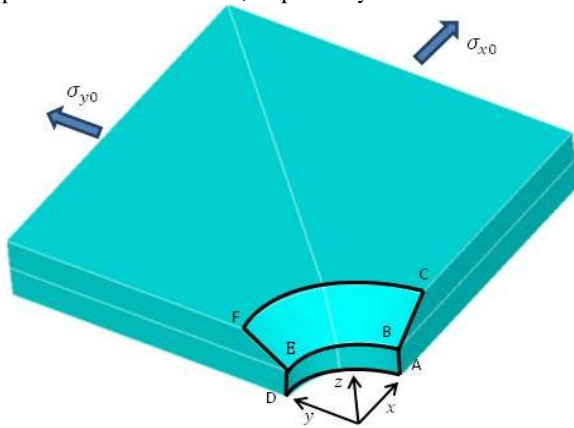


Figure 4. Paths of interest along the edges of the countersunk hole

4. Stress concentration and constraint factors' equations

The SCF is normally defined as the ratio of an elevated local stress due to stress risers to the nominal applied remote stress σ_0 . As shown previously in Fig. 1, the plate under consideration is subject to biaxial remote stresses σ_{x0} and σ_{y0} in the *x*- and *y*-directions respectively, for which, the biaxial stress ratio *R* is defined as,

$$R = \frac{\sigma_{x0}}{\sigma_{y0}} \tag{1}$$

Accordingly, in this research, the directional pointwise normal SCF $k_i(z)$ along paths *ABC* and *EDF* are defined in terms of the corresponding local normal stresses $\sigma_i(z)$ and the *y*-direction applied stress σ_{y0} as,

$$k_i(z) = \frac{\sigma_i(z)}{\sigma_{oy}}, \quad i = x, y, z \tag{2}$$

In the above equation, *z* determines a point location through the thickness of the plate at paths *ABC* or *EDF*. Similarly, the SCF at any point on the circular paths *AE*, *BD*, and *CF* is defined as,

$$k_i(\phi) = \frac{\sigma_i(\phi)}{\sigma_{yo}}, \quad i = x, y, z, \tag{3}$$

where the angle ϕ defines the angular position of any point along a specific circular path and it is measured from the *y*-axis as follows:

$$\phi = \tan^{-1} \left(\frac{x}{y} \right) \tag{4}$$

In addition, Von Mises stress concentration factor is defined as,

$$k_v(j) = \frac{\sigma_v(j)}{\sigma_{yo}}, \quad (j = z, \phi) \tag{5}$$

The maximum value of k_i along a certain path of interest specifies the stress concentration factor $k_{i,t}$ for that path. Consequently, the maximum of all $k_{i,t}$'s of the prescribed five paths is considered the stress concentration factor k_t of the hole.

The stress constraint factor $C(z)$ is in the 3-D stress analysis of solid structures characterizes the influence of the out-of-plane stress σ_z in a tri-axial stress state and contributes to the fracture mechanics analysis. This factor is defined as,

$$C(z) = \frac{\sigma_z(z)}{v[\sigma_x(z) + \sigma_y(z)]} \tag{6}$$

According to the above definition, the value of $C(z)$ ranges between 0 and 1 for plane stress and plane strain states respectively.

5. Finite element results and discussion

Tremendous number of FE runs was performed to accommodate the results of a wide range of the geometric parameters (*W/r*, *t/r*, *C_s/t*) and the biaxial loading ratio (*R*). For this purpose, the ratio of the thickness of the plate to the *SS* bore radius *t/r* was varied from 0.1 (plane stress) to 12 (plane strain), the countersink depth to thickness ratio *c_s/t* was varied from 0 (cylindrical hole) to 1 (knife edge hole) with an increment of 0.05. Similarly, the load ratio *R* was varied from 0 (uniaxial) to 1 (symmetric biaxial) with an increment of 0.25. The plate was considered square (*W* = *L*) with a width to bore radius ratio *W/r* less than 15 (finite size) or greater than 15 (infinite plate) to eliminate the size effect of the plate on the results. Finally, the countersink angle θ_c was maintained constant at the common industrial value of 100°. For each geometric and loading configuration the automated APDL ANSYS batch code defined the five paths of the countersunk hole and stored for each path the three normal stresses, σ_x , σ_y and σ_z and Von Mises stress σ_v .

6. Path ABC

Fig. 5 presents the effect of the biaxial load ratio *R* on the local SCF $k_y(z)$ for an infinite plate (*w/r* = 30) of thickness defined by the parametric ratio *t/r* = 0.1, and for countersunk holes of bound values *c_s/t* = 0 (regular hole) and *c_s/t* = 1 (knife edge hole). It is shown in

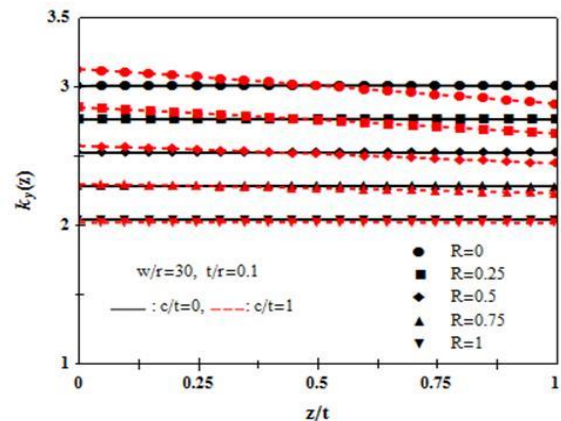


Figure 5. Effect of load ratio *R* and countersink ratio *c_s/t* on $k_y(z)$ along path *ABC* of plane stress problem/*r* = 0.1

Fig. 5 that for the regular hole, the value of $k_{y,t}$ is found equal to 3 when $R = 0$ and decreases monotonically to 2 as R increases to one which agrees with the theory of elasticity for plane stress state. It is also shown that $k_y(z)$ of the knife edge hole has insignificantly varied from that of the regular hole with $k_{y,t}$ located at the knife edge of the hole. The inverse proportionality between $k_y(z)$ and R can be explained qualitatively as illustrated in Fig. 6, when $R = 0$, the resultant force (F) of the force lines interrupted by the hole is reacted in the y -direction at point A by an equivalent resultant force (F_A) and moment (M_A) in order to maintain equilibrium and compatibility of the plate. On the other hand, by increasing the biaxial load ratio R , the reaction moment of the force lines in the x -direction would counter acts and partially cancels the moment of the main load at point A. Accordingly, when $R = 1$, the reaction moments due to the lever action are cancelled completely, hence, the value of $k_{i,t}$ is minimum.

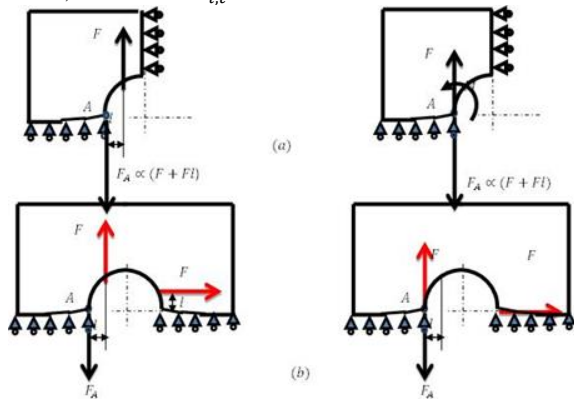


Figure 6. a) $R = 0$, and b) $R = 1$

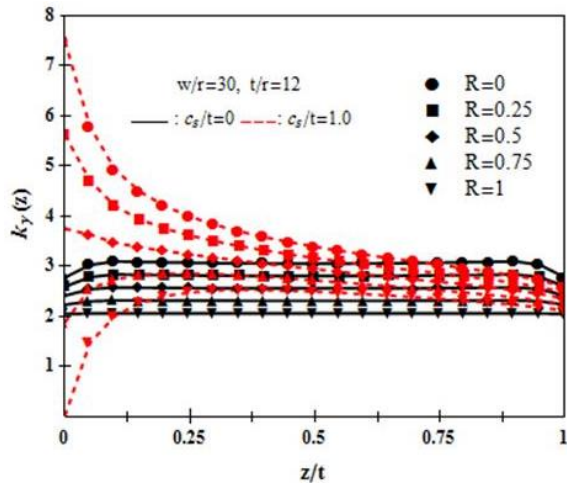


Figure 7. Effect of load ratio R and countersink ratio c_s/t , on $k_y(z)$ along path ABC of plane strain problem $t/r = 12$

Fig. 7 presents the effect of R on $k_y(z)$ for a thick plate ($t/r = 12$) for two cases, $c_s/t = 0$ and $c_s/t = 1$. When $c_s/t = 0$, the results are pretty much similar to those of Fig. 5 with a slight difference at the edges of the hole which reflects the plane strain effect on the stress state. However, for $c_s/t = 1$, the trend of $k_y(z)$ has dramatically changed compared to that of Fig. 5 while maintaining the inverse relationship between R and $k_y(z)$. Here it is observed that the effect of R on the SCF is more

significant at the sharp edge side of the hole at $z/t=0$ than on the other side at $z/t=1$. It is also found that the SCF at the sharp edge switches from maximum value when $R = 0, 0.25$ and 0.5 to a minimum value when $R = 0.75$ and 1 , and that it equals to zero at $R=1$. This result is quite surprising, but it can be referred to the fact that as we increase the thickness of the plate the plane strain effect and hence the transverse stress σ_z which compressive in our case become more pronounced. From mechanics point of view, the resultant force of the transverse stresses in the vicinity of the knife edge hole when $R=1$ will create compressive moment stress at the sharp edge of the hole that counter acts the applied tension stress and therefore the SCF would be reduced. Fig. 8 presents how the SCF decreases at the sharp edge of the knife edge hole ($z/t=0$) as t/r increases and for $R=1$.

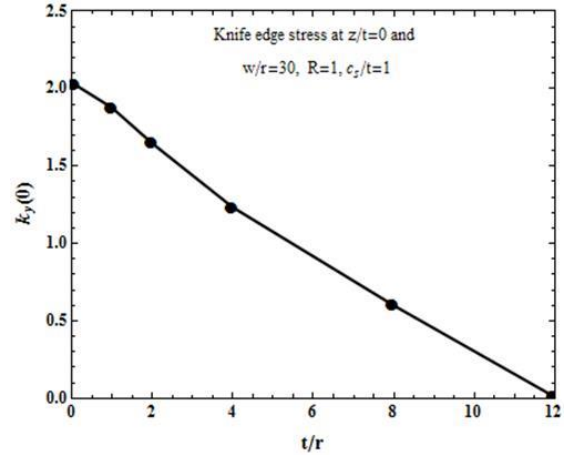


Figure 8. The values of the stress concentration at $z/t = 0$ and $R = 1$.

In Figs 9 and 10 different values of c_s/t (0.25, 0.5, 0.75) are considered to examine the distributions of $k_y(z)$ and $k_v(z)$ respectively for countersunk holes in infinite plates with $t/r = 12$. Both Figs show similar trends with maximum values of $k_v(z)$ and $k_y(z)$ at the

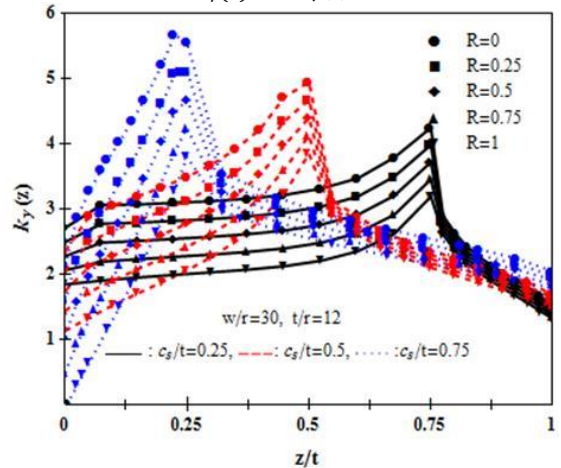


Figure 9. Effect of load and countersink ratios on $k_y(z)$ along path ABC of plane strain problem $t/r = 12$.

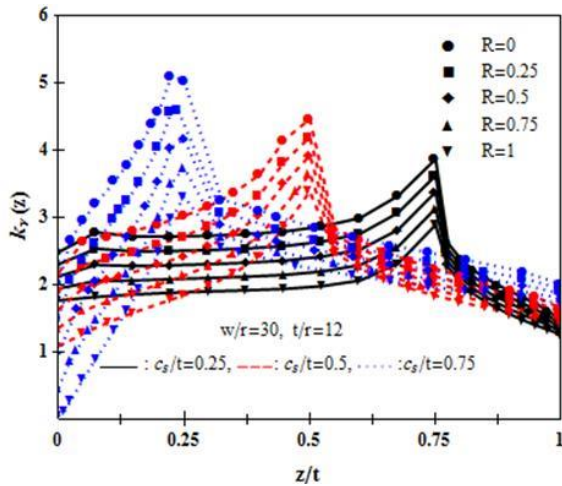


Figure 10. Effect of load ratio R on Von misses stress concentration factor $k_y(z)$ along path ABC, $t/r = 12$

countersink edge ($z/t = b/t$). Figs. 11 and 12 present the effect of the load ratio R on $k_y(z)$ of an infinite plate of thickness ratio $t/r = 1$ for different values of c_s/t .

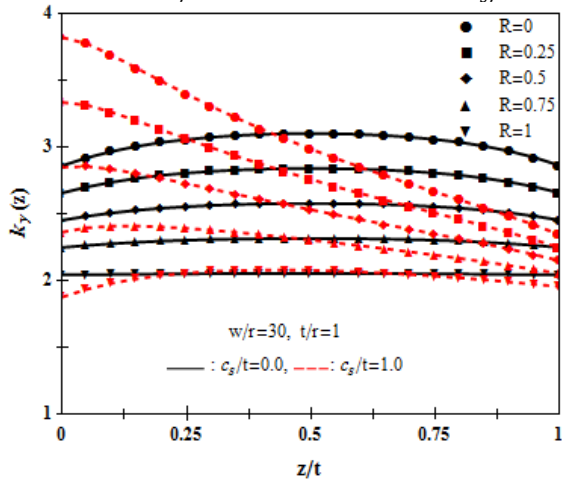


Figure 11. Effect of load ratio R on $k_y(z)$ along path ABC, $t/r = 1$

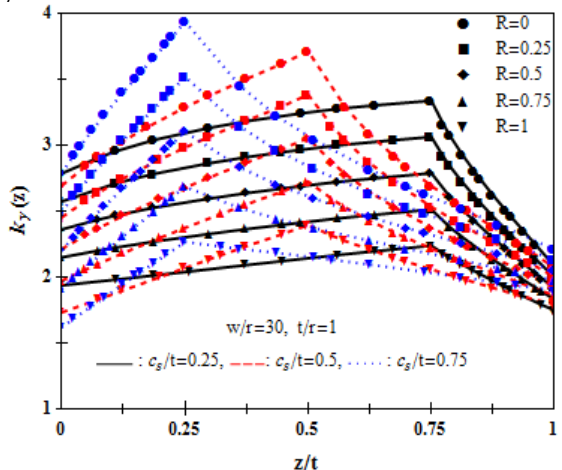


Figure 12. Effect of load ratio R on $k_y(z)$ along path ABC, $t/r = 1$

Figs 13 and 14 present the variations of $k_{y,t}$ and $k_{v,t}$ respectively with increasing the loading ratio R for a wide range of plate thicknesses ($t/r=0.1-2.4$) and for finite and infinite width plates

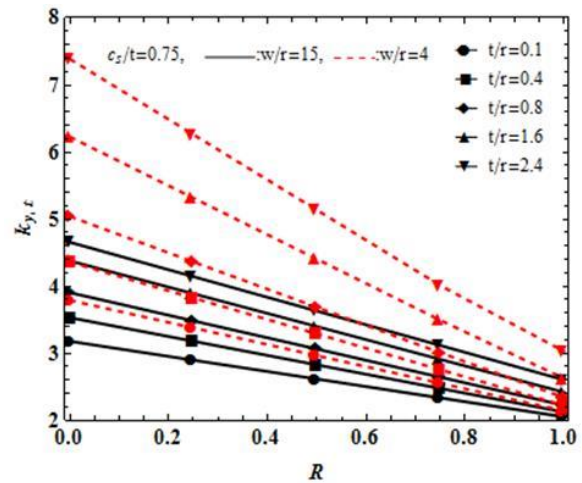


Figure 13. Effect of load ratio R on $k_{y,t}$ for two different bore radius (w/r) and various values of thicknesses (t/r)

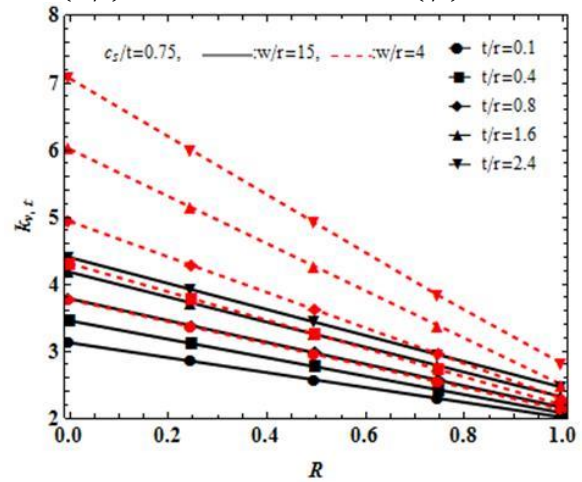


Figure 14. Effect of load ratio R on $k_{v,t}$ for two different bore radius (w/r) and various values of thicknesses (t/r).

($w/r = 4$ and 15 respectively). The two Figs show that the maximum SCF ($k_{y,t}$ or $k_{v,t}$) decreases with increasing R , with increasing the plate's width, and with decreasing the plate's thickness.

The transverse variation of the stress constraint factor $C(z)$ which is expressed in Eq. (6) is shown in Figs 15 for two cases; a regular hole ($c_s/t = 0$) and a knife edge hole ($c_s/t = 1$). It is shown that for $c_s/t = 0$, $C(z)$ decreases monotonically with increasing R . This relationship is linked to the faster rate of decreasing σ_z (in the numerator of $C(z)$) than the sum of σ_x and σ_y (in the denominator of $C(z)$) around the hole with increasing R . On the other hand, for $c_s/t = 1$, the relationship is reversed such that $C(z)$ increases with increasing R . This reversal in the relationship between $C(z)$ and R is referred to the tapered geometry of the knife edge hole which in turns affects the tri-axial stress distributions around the hole. As a result, σ_z tends to increase with increasing R and therefore the ratio $C(z)$ increases. Fig. 16 shows the effect of R on σ_z and $\nu(\sigma_x + \sigma_y)$ for both regular and knife edge holes. It is also shown in Fig. 15 that the values of $C(z)$ of a knife-edge hole are smaller than those of a regular hole. For countersunk holes with intermediate values of c_s/t (0.25, 0.5, 0.75), the transverse distribution of $C(z)$ at different R values is shown in Fig. 17. It is shown that the relationship between $C(z)$ and R within the straight shank and sinking portions of the hole is similar to that of the

regular hole and the knife edge hole respectively. The maximum value of $C(z)$ occurs just below the countersunk root in the straight shank part.

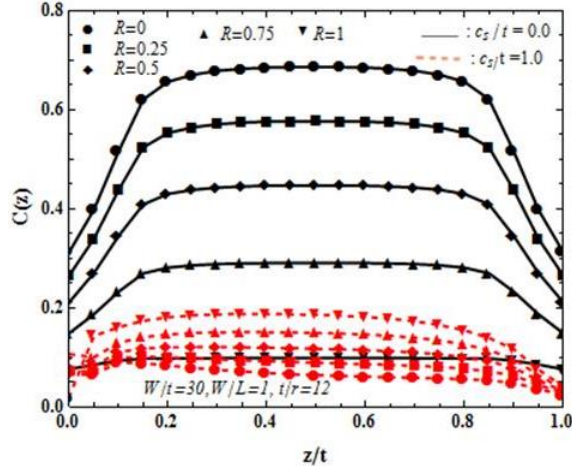


Figure 15. Effect of load ratio R on $C(z)$ for two values of (C_s/t)

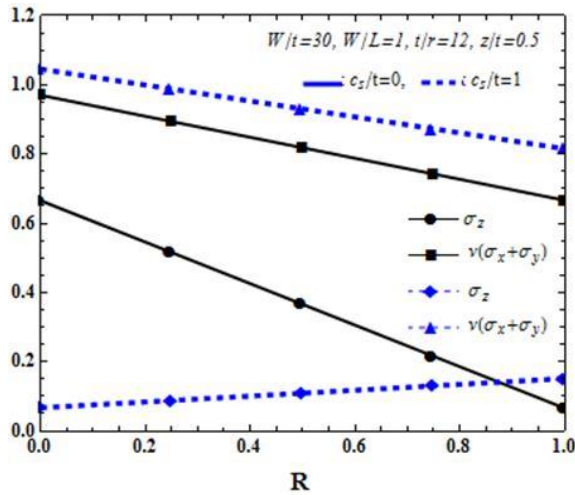


Figure 16. Effect of the biaxial load ratio R on σ_z and $v(\sigma_x + \sigma_y)$

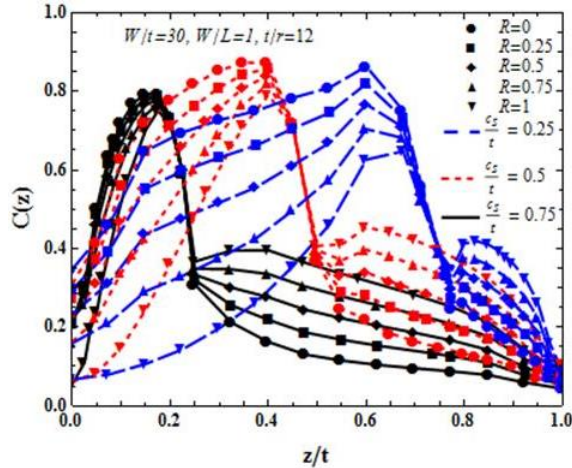


Figure 17. Effect of load ratio R on $C(z)$ for three values of (C_s/t)

Fig. 18 shows that the maximum stress constraint factor C_{max} increases when the thickness of the plate (t/r) increases, and that it approaches zero for very thin plates i.e. $t/r = 0.1$. It is also noticed that C_{max} is greater in value in countersunk holes with c_s/t falling in general between 0.25 and 0.5 than the other hole configurations.

Due to geometrical symmetry of the plate and the hole, any further investigations of the stress concentration factors and the stress constraint factor along the path DEF would be redundant.

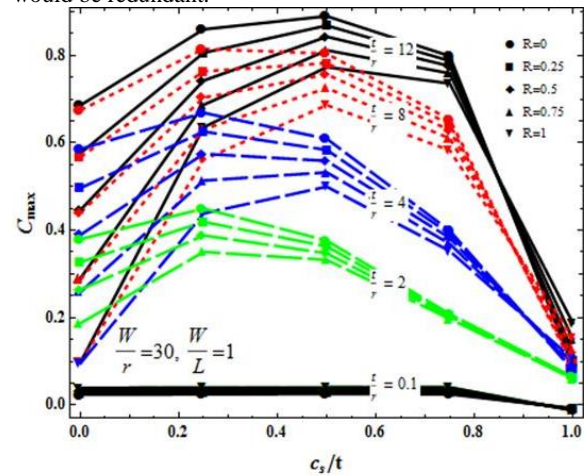


Figure 18. Effect of load ratio R on C_{max}

7. Paths AD, BE and CF

The circular paths AD , BE and CF are defined at the intersections of the countersunk hole surface with the x - y planes at $z=0$, $z=b$, and $z=t$, respectively. Figs 19-21 show the circumferential distribution of the local stress concentration factors $k_y(\phi)$ along path BE for countersunk holes with $(c_s/t = 0.25, 0.5, 0.75)$, along path AD for regular and knife edge holes, and along path CF for regular and knife edge holes respectively in infinite and thick plates at different R values.

From Figs. 19 and 21, it is found that the angular position of the maximum stress concentration factor is at $\phi = \pi/2$. It is also noticed that, in general, for each value of (c_s/t) there is a common deflection point (or angle) for the set of curves of different R values below which the relation between k_y and R is in directly proportionality and beyond which the relation gets reversed.

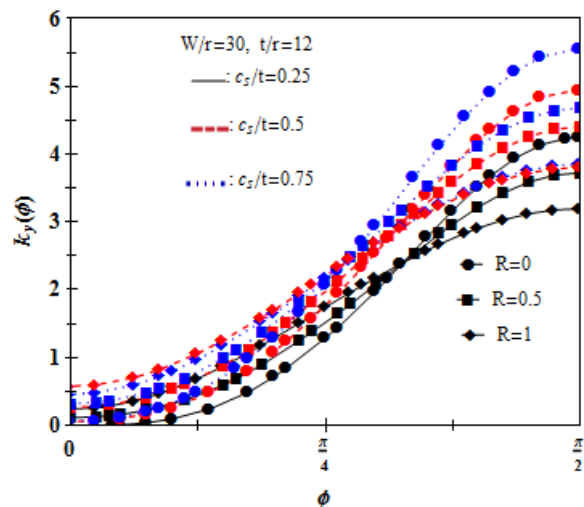


Figure 19. Effect of load ratio R on $k_y(z)$ along path BE , $t/r = 12$.

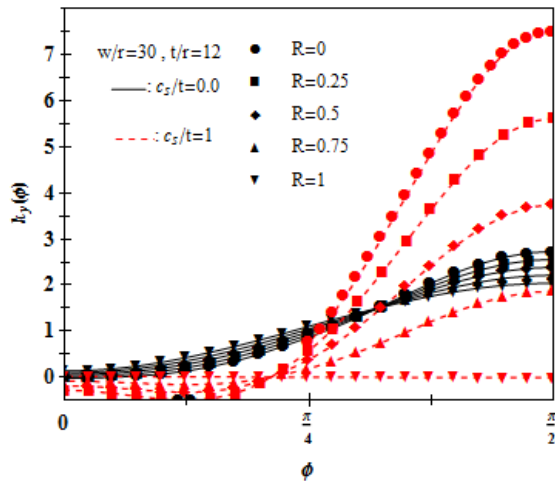


Figure 20. Effect of load ratio R on $k_y(z)$ along path AD, $t/r = 12$.

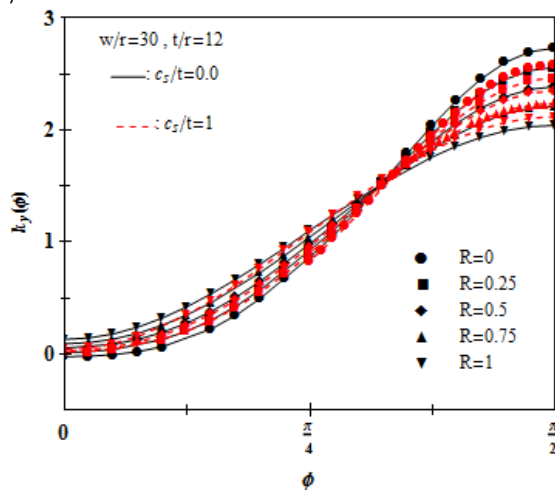


Figure 21. Effect of load ratio R on $k_y(z)$ along path CF, $t/r = 12$.

8. Conclusion

The effect of the biaxial loading ratio R on the magnitudes and locations of the local and global stress concentration factors k_i and $k_{i,t}$, ($i = y, v$) were investigated along the prescribed five paths of the countersunk hole. As may be anticipated, the increase of the biaxial loading ratio R was found to decrease monotonically the magnitude of k_i , yet magnitudes of $k_{i,t}$ have decreased linearly with increasing R for all considered values of c_s/t and t/r . In addition, the location of the maximum stress concentration k_t was found to be at the root of the countersunk hole at $z = b$ and at an angular location $\phi = \pi/2$. It was also found that at the sharp corner of a knife edge hole the SCF can drop from a maximum value for thin plate (plane stress) when subjected to a uniaxial load to a minimum value that can reach zero for a very thick plate (plane strain) under symmetric biaxial loading.

The study was further extended to examine the influence of the biaxial loading ratio R and the hole geometry on the generated transverse stress σ_z represented by the dimensionless stress constraint factor surrounding the hole. It was found that the magnitude of the local stress constraint factor $C(z)$ attained a severe jump at the root of the countersunk hole ($z=b$), and its maximum value C_{max}

occurred always at the straight shank part of the hole. The maximum stress constraint factor C_{max} was also found a function of c_s/t where in general it attains its maximum value when c_s/t falls between 0.25 and 0.5. Finally, the relationship between the stress constraint factor and the load ratio was found to be in direct proportionality in straight regular holes and that it got reversed in knife edge holes.

References

- [1] Pilkey, W.D., Pilkey, D.F., 2008. Peterson's Stress Concentration Factors, third ed. John Wiley & Sons, New York.
- [2] Isaac M. Daniel, 1980. Behavior of graphite/epoxy plates with holes under biaxial loading. *Experimental Mechanics*, 20 (1), 1-8.
- [3] Isaac M. Daniel, 1982. Biaxial testing of $[O_2/\pm 45]_s$ graphite/epoxy plates with holes. *Experimental Mechanics*, 22 (5), 188-195.
- [4] Dharmendra S Sharma, 2011. Stress concentration around circular/elliptical/triangular cutouts in infinite composite plate. *Proceedings of the World Congress on Engineering Vol III WCE*, London, U.K.
- [5] G.H. Rahimi, R.A. Alashti, 2005. Limit load analyses of plates with a hole under in-plane loads. *Scientia Iranica*, 12 (4), 442-454.
- [6] Xin-Lin Gao, 1996. A general solution of an infinite elastic plate with an elliptic hole under biaxial loading. *The International Journal of Pressure Vessels and Piping*, 67 (1), 95-104.
- [7] H. Vlieger, H.H. Ottens, 1998. Uniaxial and biaxial tests on riveted fuselage lap joint specimens. *FAA Final Report*, DOT/FAA/AR-98/33.
- [8] A.K.L. Srivastava, P.K. Datta, 2006. Elastic stability of square stiffened plates with cutouts under biaxial loading. *Int. J. of Applied Mechanics and Engineering*, 11 (2), 421-433.
- [9] Wharely, R. E., 1965. Stress-concentration factors for countersunk holes. *Experimental Mechanics*, 5 (8), 257-261.
- [10] Shivakumar, K.N., Newman, J.C., 1992. Stress concentrations for straight-shank and countersunk holes in plates subjected to tension, bending, and pin loading. *NASA Technical Paper 3192*.
- [11] Shivakumar, K.N., Bhargava, A., Hamoush, S., 2007. A general equation for stress concentration in countersunk holes. *CMC*, 6 (2), 71-92.
- [12] Bhargava, A., Shivakumar, K.N., 2008. A three dimensional strain concentration equation for countersunk holes. *Journal of Strain Analysis for Engineering Design*, 43 (2), 75-85.
- [13] Darwish, F., Gharaibeh, M., Tashtoush, G., 2012. A modified equation for the stress concentration factor in countersunk holes. *European Journal of Mechanics - A/Solids*, 36, 94-103.
- [14] Feras Darwish, Ghassan Tashtoush, Mohammad Gharaibeh, 2013. Stress concentration analysis for countersunk rivet holes in orthotropic plates. *European Journal of Mechanics - A/Solids*, 37, 69-78.
- [15] Wu, H., Mu, B., 2003. On stress concentrations for isotropic/orthotropic plates and cylinders with a circular hole. *Composites: Part B*, 34 (2), 127-134.
- [16] Feras Darwish, Lubna Al-Nasser, Omar Al-Araidah, 2013. Tensile stress concentration in plates with double countersunk rivet holes. *Int. J. Design Engineering*, Accepted in-press.
- [17] Kotousov, A., Wang, C.H., 2002. Three-dimensional stress constraint in an elastic plate with a notch. *International Journal of Solids and Structures*, 77, 1665-1681.
- [18] Kotousov, A., Lazzarin, P., Berto, F., Harding, S., 2010. Effect of the thickness on elastic deformation and quasi-

- brittle fracture of plate components. *Engineering Fracture Mechanics*. 39, 4311-4326.
- [19] Li, .Z., Guo, W., Kuang, Z., 2000. Three-dimensional elastic stress fields near notches in finite thickness plates. *International Journal of Solids and Structures*. 37, 7617-7631.
- [20] Berto, F., Lazzarin, P., Wang, C.H., 2004. Three-dimensional linear elastic distributions of stress and strain energy density ahead of V-shaped notches in plates of arbitrary thickness. *International Journal of Fracture*. 127, 265-282.
- [21] She, C., Guo, W., 2007. Three-dimensional stress concentrations at elliptic holes in elastic isotropic plates subjected to tensile stress. *International Journal of Fatigue*. 29, 330-335.